



Article

Semi-analytical Solution for Surface Coverage Model in an Electrochemical Arsenic Sensor Using a New Approach to Homotopy Perturbation Method

*V. Ananthaswamy¹, S. Narmatha²

¹Department of Mathematics, The Madura College, Madurai, Tamil Nadu, India.

²Department of Mathematics, Lady Doak College, Madurai, Tamil Nadu, India

*Author to whom correspondence should be addressed; E-Mail: ananthu9777@rediffmail.com

Article history: Received 5 June 2019; Revised 7 July 2019; Accepted 7 July 2019; Published 24 July 2019.

Abstract: The theoretical model for the surface coverage parameter of an electrochemical sensor is considered and discussed. Semi-analytical solution has been derived for arsenic concentration in the steady state and the non-steady state using a new approach to Homotopy perturbation method. Upon comparison, we found that the analytical results of this work are in excellent agreement with the numerical results. Further, the sensitivity of the parameters in the diffusion of the arsenic ions was also analyzed due to its importance in predicting the relationship between the parameters and the model results.

Keywords: Reaction-diffusion equations; Surface coverage; Michaelis – Menten constant; Sensitivity analysis; New Homotopy perturbation method; Numerical simulation.

Mathematics Subject Classification: 34E, 35K20 and 68U20

1. Introduction

Arsenic contamination of groundwater in different parts of the world is an outcome of natural and/or anthropogenic sources, leading to adverse effects on human health and ecosystem. Millions of people from different countries are heavily dependent on groundwater containing elevated level of $[As]$ for drinking purposes. $[As]$ contamination of groundwater, poses a serious risk to human health.

Excessive and prolonged exposure of inorganic $[As]$ with drinking water is causing arsenicosis, a deteriorating and disabling disease characterized by skin lesions and pigmentation of the skin, patches on palm of the hands and soles of the feet. Arsenic poisoning culminates into potentially fatal diseases like skin and internal cancers [2].

In the proposed model [1], Michaelis - Menten kinetics, which represents the enzymatic reaction, has been included as a nonlinear term in the differential equation. The computational modelling is widely used instead of expensive physical experiments aiming at understanding the kinetic peculiarities of the sensors [3]. Sensors are analytical devices utilized for the recognition of chemical substances in a solution to be analyzed. Computational modelling is widely used to improve the sensors design and to optimize their configuration [4]. The mathematical modelling of sensors is complicated and time-consuming task [5]. Surface coverage parameter of an electrochemical sensor plays a vital role in enhancing the figure of merits of the sensor. Developing a theoretical model for the surface coverage will help to standardize the fabrication of working electrodes used in electrochemical sensors. In this background, a wavelet based spectral algorithm was developed to model the surface coverage of an arsenic sensor [1].

2. Mathematical Formulation of the Problem

Sathiyaseelan et al.[1] developed the differential mass balance for arsenic in the case of arsenic-F-doped CdO catalytic reaction, in an unsteady state as follows

$$\frac{\partial [As]}{\partial t} = D_{[As]} \frac{\partial^2 [As]}{\partial x^2} - \frac{I_{\max} [As]}{K_M + [As]} \quad (1)$$

where $[As]$ is the arsenic concentration, $D_{[As]}$ is the diffusion coefficient of arsenic, t is time, x is the thickness of the F-doped CdO thin film electrode, I_{\max} is the maximum current response and K_M is the Michaelis - Menten constant. In their work, the diffusion layer was defined as the region in the vicinity of F-doped CdO thin film electrode where the concentration of arsenic is different from its value in the bulk solution (0.4 M NaCl).

Sathiyaseelan et al.[1] have given the boundary conditions for the arsenic sensor are as follows

$$x = 0, \frac{\partial [As]}{\partial t} = 0 \text{ (no transport of arsenic ion)}$$

$$x = d, As = A_{s_0} \text{ (insignificant liquid film resistance)}$$

$$t = 0, [As] = 0 \text{ (arsenic diffusion not in progress)}$$

However, we see that $x = 0, \frac{\partial[As]}{\partial t} = 0$ is not possible, since, in that case the entire system would change into steady state, and (1) would become independent of time. Furthermore, the authors have used $\left(\frac{d[As]}{dx}\right)_{x=0} = 0$ in the latter part of the paper. Hence, we have considered the following conditions as boundary conditions for the arsenic sensor

$$x = 0, \frac{\partial[As]}{\partial x} = 0 \text{ (no transport of arsenic ion)} \tag{2}$$

$$x = d, [As] = A_{s_0} \text{ (insignificant liquid film resistance)} \tag{3}$$

$$t = 0, [As] = 0 \text{ (arsenic diffusion not in progress)} \tag{4}$$

Introduce the following dimensionless variables

$$A = \frac{[As]}{A_{s_0}}, X = \frac{x}{d}, \tau = \frac{D_{[As]}t}{d^2} \tag{5}$$

Hence we get

$$\frac{\partial[As]}{\partial t} = \left(\frac{A_{s_0}D_{[As]}}{d^2}\right) \frac{\partial A}{\partial \tau} \tag{6}$$

$$\frac{\partial[As]}{\partial x} = \left(\frac{A_{s_0}}{d}\right) \frac{\partial A}{\partial X} \tag{7}$$

$$\frac{\partial^2[As]}{\partial x^2} = \left(\frac{A_{s_0}}{d^2}\right) \frac{\partial^2 A}{\partial X^2} \tag{8}$$

Substituting the eqns. (6) to (8) in an eqn. (1), we get

$$\frac{\partial A}{\partial \tau} = \frac{\partial^2 A}{\partial X^2} - \frac{d^2 I_{\max}}{A_{s_0} D_{[As]}} \left(\frac{A}{\frac{K_M}{A_{s_0}} + A} \right) \tag{9}$$

Introduce $\phi^2 = \frac{d^2 I_{\max}}{A_{s_0} D_{[As]}}$, $\alpha = \frac{K_M}{A_{s_0}}$ (10)

The eqn.(8) becomes

$$\frac{\partial A}{\partial \tau} = \frac{\partial^2 A}{\partial X^2} - \phi^2 \left(\frac{A}{\alpha + A} \right) \tag{11}$$

The boundary conditions (2) to (4) become

$$X = 0, \frac{\partial A}{\partial X} = 0 \tag{12}$$

$$X = 1, A = 1 \tag{13}$$

$$\tau = 0, A = 0 \tag{14}$$

3. New Approach to Homotopy Perturbation Method

Linear and non-linear differential equations can model many phenomena in different fields of Science and Engineering in order to present their behaviors and effects by mathematical concepts. Most of the non-linear differential equations do not have analytical solutions which can be handled by semi-analytical or numerical methods. In order to obtain exact solution of non-linear differential equations, semi-analytical methods such as the variational iteration method[6], Homotopy perturbation method[7], Homotopy analysis method[8], and a new approach to the Homotopy perturbation method[9] are considered.

The Homotopy perturbation method was developed by He [10-15]. It is used to solve a system of linear and nonlinear differential equations to determine an approximate solution of the system. The Homotopy perturbation method [16] has been applied to several initial and boundary value problems. Lately, a new approach to HPM is used to solve nonlinear differential equation in zeroth iteration [15].

4. Semi-analytical Solution to the Steady State of Eqns. (1) to (4) Using New Approach to Homotopy Perturbation Method

Using new approach to HPM [17-24], the solution of the eqns. (11) to (14) in steady state is as follows:

$$A = \frac{\cosh \frac{\phi}{\sqrt{\alpha + 1}} X}{\cosh \frac{\phi}{\sqrt{\alpha + 1}}} \tag{15}$$

Using the eqns.(5) and (10) in an eqn. (15), we get the steady state solution to the eqns. (1) to (4) is as follows:

$$[As] = \frac{\cosh\left(\sqrt{\frac{I_{\max}d^2}{As_0D_{[As]}\left(\frac{K_M}{As_0} + 1\right)}}x\right)}{\cosh\left(\sqrt{\frac{I_{\max}d^2}{As_0D_{[As]}\left(\frac{K_M}{As_0} + 1\right)}}\right)} \tag{16}$$

5. Semi-analytical Solution to Eqns. (1) to (4) (non-steady state) Using New Approach to Homotopy Perturbation Method

Using new approach to HPM and Laplace transform technique [25-27], the solution to the eqns. (1) to (4) in the non- steady state is evaluated as follows:

$$A \approx A_0 = \frac{\cosh\frac{\phi}{\sqrt{\alpha+1}} X}{\cosh\frac{\phi}{\sqrt{\alpha+1}}} + \sum_{n=0}^{\infty} \frac{(-1)^{n+1} (2n+1)\pi \cos\left(\frac{2n+1}{2} \pi X\right) e^{-\left(\frac{\phi^2}{\alpha+1} + \frac{(2n+1)^2 \pi^2}{4}\right)\tau}}{\frac{\phi^2}{\alpha+1} + \frac{(2n+1)^2 \pi^2}{4}} \tag{17}$$

Using the eqns.(5) and (10) in an eqn. (17), we get the non-steady state solution to the eqns. (1) to (4) is as follows:

$$[As] = \frac{\cosh\left(\sqrt{\frac{I_{\max}d^2}{As_0D_{[As]}\left(\frac{K_M}{As_0} + 1\right)}}x\right)}{\cosh\left(\sqrt{\frac{I_{\max}d^2}{As_0D_{[As]}\left(\frac{K_M}{As_0} + 1\right)}}\right)} + \sum_{n=0}^{\infty} \frac{(-1)^{n+1} (2n+1)\pi \cos\left(\frac{(2n+1)\pi x}{2d}\right) e^{-\left(\frac{I_{\max}d^2}{As_0D_{[As]}\left(\frac{K_M}{As_0} + 1\right)} + \frac{(2n+1)^2 \pi^2}{4}\right)\frac{D_{[As]}t}{d^2}}}{\frac{I_{\max}d^2}{As_0D_{[As]}\left(\frac{K_M}{As_0} + 1\right)} + \frac{(2n+1)^2 \pi^2}{4}} \tag{18}$$

The steady state of the eqns. (17) and (18) are as follows:

$$A_\infty = \frac{\cosh\frac{\phi}{\sqrt{\alpha+1}} X}{\cosh\frac{\phi}{\sqrt{\alpha+1}}} \tag{19}$$

$$[As]_\infty = \frac{\cosh\left(\sqrt{\frac{I_{\max}d^2}{As_0 D_{[As]} \left(\frac{K_M}{As_0} + 1\right)}} x\right)}{\cosh\left(\sqrt{\frac{I_{\max}d^2}{As_0 D_{[As]} \left(\frac{K_M}{As_0} + 1\right)}}\right)} \tag{20}$$

We here note that eqns. (19) and (20) exactly coincide with eqns. (15) and (16) respectively. This clearly indicates that the solution derived for the non-steady state converges to the solution derived for the steady state as $t \rightarrow \infty$.

6. Numerical Simulation

The non-linear reaction diffusion eqn. (11) with respect to the initial and boundary conditions (12) to (14) is also solved numerically. The function pde4 has been used in MATLAB software to solve the initial-boundary value problem numerically. The obtained analytical results are compared with the numerical simulation. The numerical results are presented in figures and tables below. The MATLAB program is given in Appendix D.

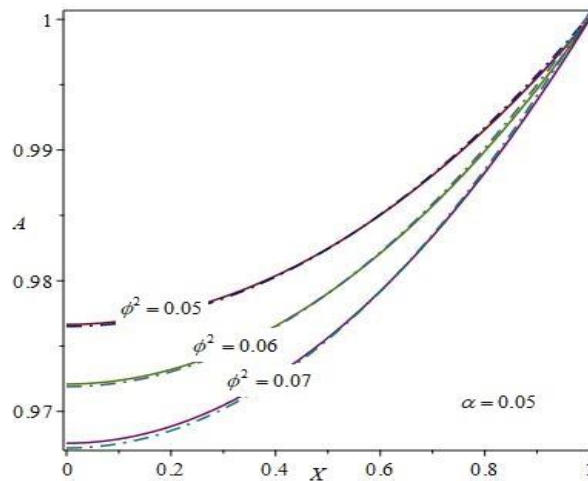


Fig. 1: Plot of dimensionless concentration of arsenic (A) versus dimensionless thickness of the F-doped CdO electrode(X) for some fixed values of parameters and various values of ϕ^2 . The lines with dots and dashes represent analytical solution and solid lines represent the numerical simulation.

Table 1: Comparison between analytical values and numerical values in Fig. 1

$\alpha = 0.05$				
ϕ^2	X	Numerical solution for A	Analytical solution for A	Absolute percentage error
0.05	0	.9765	.9766539125	0.015762
	0.2	.9774512874	.9775842066	0.013599
	0.4	.9803052381	.9803768615	0.007306
	0.6	.9850621170	.9850371972	0.00253
	0.8	.9917223626	.9915740932	0.01495
	1	1	1	0
0.06	0	.9719	.9720933937	0.019899
	0.2	.9730412909	.9732045694	0.01678
	0.4	.9764652947	.9765406364	0.007716
	0.6	.9821724022	.9821092209	0.00643
	0.8	.9901632597	.9899230544	0.02426
	1	1	1	0
0.07	0	.9672	.9675681499	0.038063
	0.2	.9685311750	.9688585278	0.033799
	0.4	.9725248796	.9727331022	0.021411
	0.6	.9791816498	.9792022077	0.002099
	0.8	.9885023700	.9882830999	0.02218
	1	1	1	0
Average absolute percentage error				0.01371

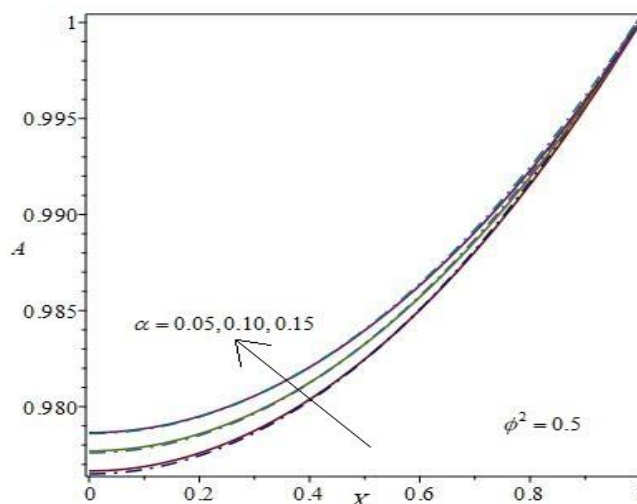


Fig. 2: Plot of dimensionless concentration of arsenic (A) versus dimensionless thickness of the F-doped CdO electrode(X) for some fixed values of parameters and various values of α . The lines with dots and dashes represent analytical solution and solid lines represent the numerical simulation.

Table 2: Comparison between analytical values and numerical values in Fig. 2

$\phi^2 = 0.5$				
α	X	Numerical solution for A	Analytical solution for A	Absolute percentage error
0.05	0	.9765	.9766539125	0.015762
	0.2	.9774512874	.9775842066	0.013599
	0.4	.9803052381	.9803768615	0.007306
	0.6	.9850621170	.9850371972	0.00253
	0.8	.9917223626	.9915740932	0.01495
	1	1	1	0
0.10	0	.9776	.9776953558	0.009754
	0.2	.9785071730	.9785843048	0.007883
	0.4	.9812288482	.9812527668	0.002438
	0.6	.9857654921	.9857055953	0.00608
	0.8	.9921178775	.9919508874	0.01683
	1	1	1	0
Average absolute percentage error				0.008094

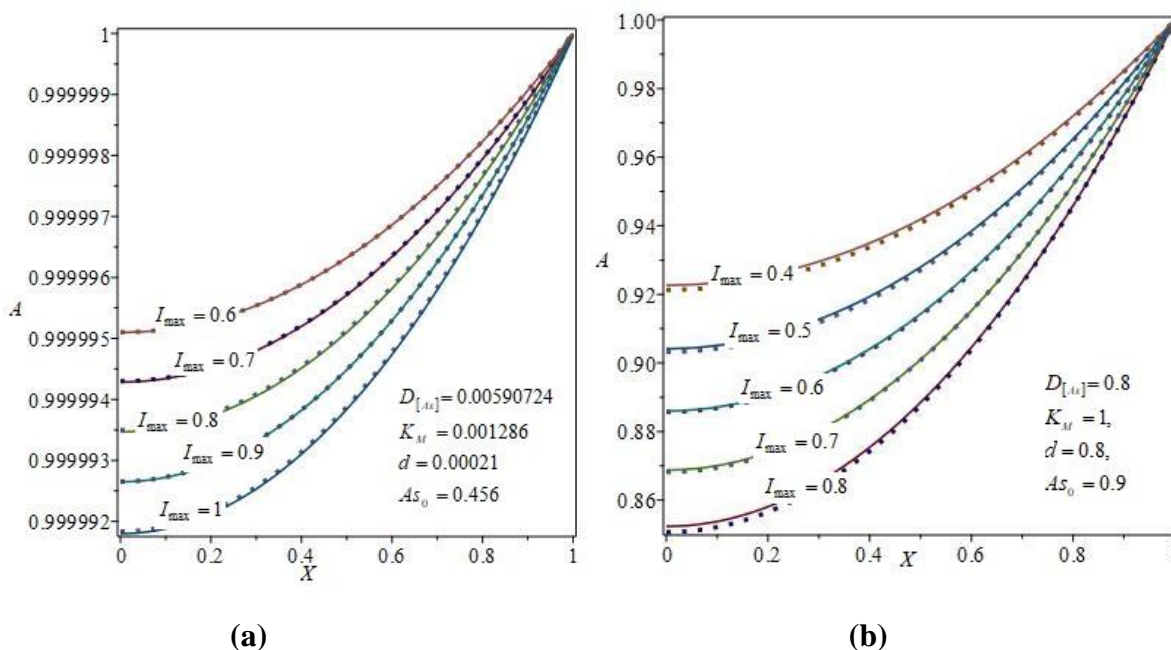


Fig. 3: (a) and (b): Plot of dimensionless concentration of arsenic (A) versus dimensionless thickness of the F-doped CdO electrode(X) for some fixed values of parameters and various values of I_{max} . The dotted lines represent analytical solution and solid lines represent the numerical simulation.

Table 3: Comparison between analytical values and numerical values in Fig. 3(b)

$D_{[As]}=0.8, K_M=1, d=0.8, As_0=0.9$				
I_{max}	X	Numerical solution for A	Analytical solution for A	Absolute percentage error
0.7	0	.86818	.8687918076	0.07047
	0.2	.8733875813	.8739181397	0.060747
	0.4	.8890435816	.8893576335	0.035325
	0.6	.9152468801	.9152924912	0.004983
	0.8	.9521593601	.9520287707	0.01372
	1	1	1	0
0.8	0	.85068	.8523680879	0.19844
	0.2	.8565672611	.8581168078	0.180902
	0.4	.8742727980	.8754405098	0.133564
	0.6	.9039265447	.9045728708	0.071502
	0.8	.9457407172	.9459068519	0.017567
	1	1	1	0
Average absolute percentage error				0.065602

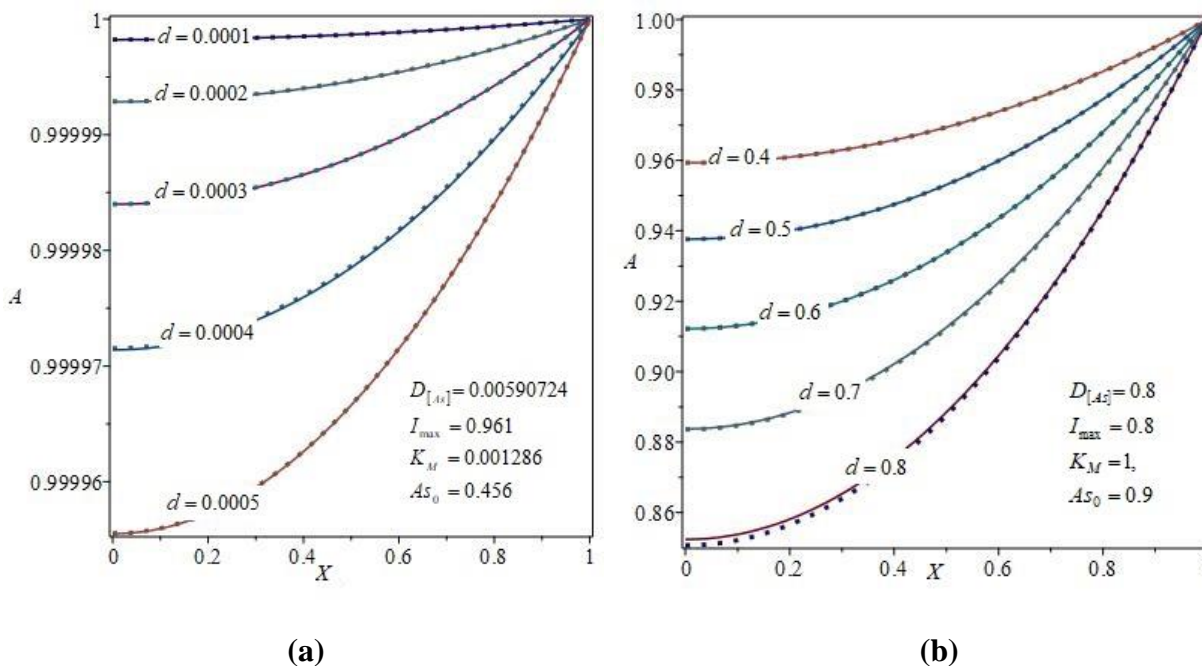


Fig. 4: (a) and (b): Plot of dimensionless concentration of arsenic (A) versus dimensionless thickness of the F-doped CdO electrode(X) for some fixed values of parameters and various values of d . The dotted lines represent analytical solution and solid lines represent the numerical simulation.

Table 4: Comparison between analytical values and numerical values in Fig. 4(b)

$D_{[As]}=0.8, I_{max}=0.8, K_M=1, As_0=0.9$				
d	X	Numerical solution for A	Analytical solution for A	Absolute percentage error
0.7	0	.88376	.8835931897	0.018875068
	0.2	.8883597145	.8881545893	0.023090331
	0.4	.9021841516	.9018858837	0.033060645
	0.6	.9253085967	.9249288437	0.041040686
	0.8	.9578565683	.9575213802	0.034993559
	1	1	1	0
0.8	0	.85067	.8523680879	0.199617701
	0.2	.8565572611	.8581168078	0.182071505
	0.4	.8742627980	.8754405098	0.134709129
	0.6	.9039165447	.9045728708	0.072609148
	0.8	.9457307172	.9459068519	0.018624192
	1	1	1	0
Average absolute percentage error				0.063224

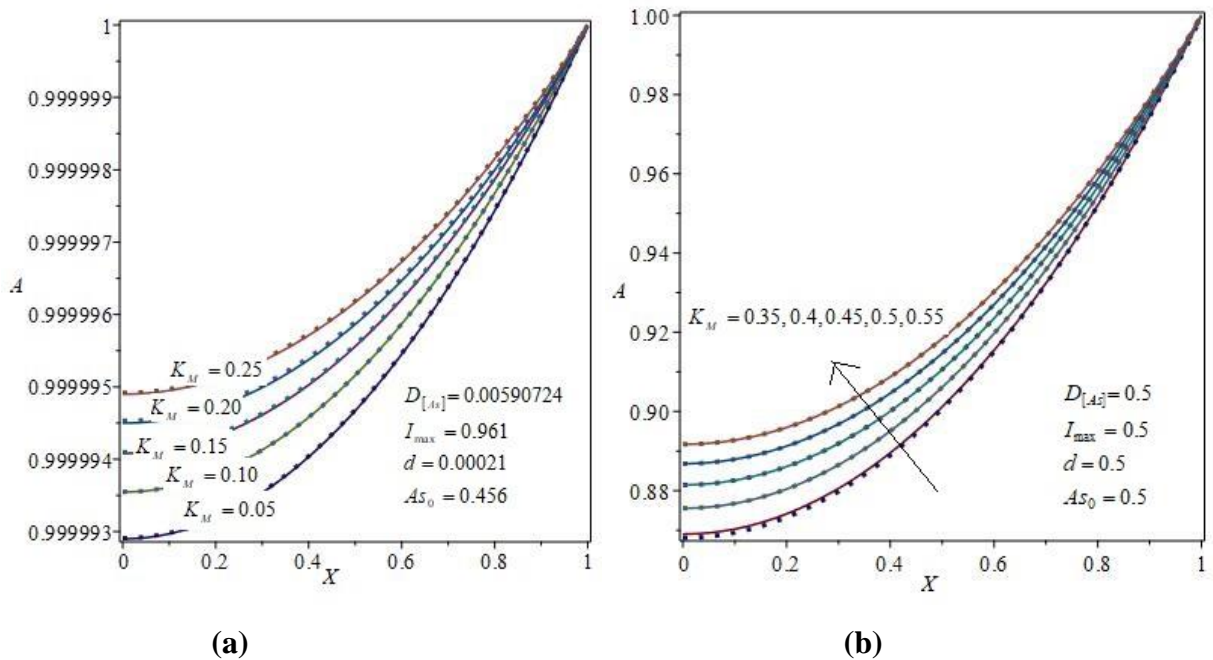


Fig. 5: (a) and (b): Plot of dimensionless concentration of arsenic (A) versus dimensionless thickness of the F-doped CdO electrode(X) for some fixed values of parameters and various values of K_M . The dotted lines represent analytical solution and solid lines represent the numerical simulation.

Table 5: Comparison between analytical values and numerical values in Fig. 5(b)

$D_{[As]}=0.5, I_{max}=0.5, d=0.5, As_0=0.5$				
K_M	X	Numerical solution for A	Analytical solution for A	Absolute percentage error
0.35	0	.8681	.8690371979	0.107959671
	0.2	.8733072906	.8741541949	0.096976667
	0.4	.8889589247	.8895654460	0.068228271
	0.6	.9151432569	.9154524364	0.03378482
	0.8	.9520045048	.9521200192	0.012133808
	1	1	1	0
Average absolute percentage error				0.053181

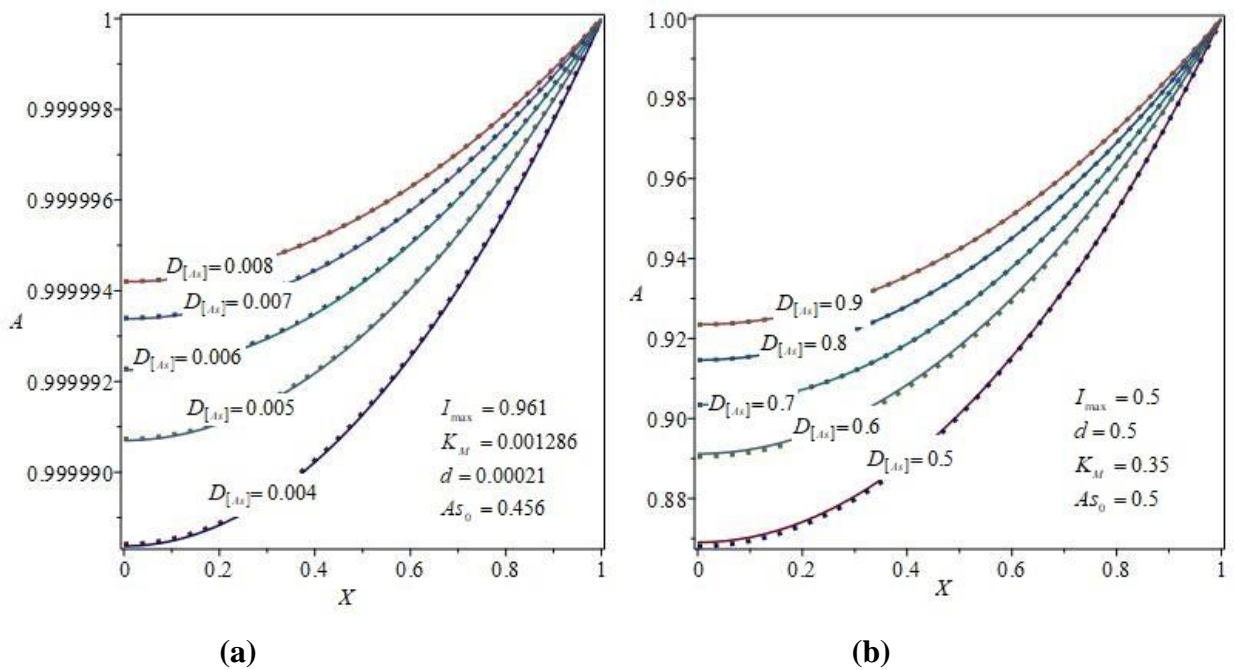


Fig. 6: (a) and (b): Plot of dimensionless concentration of arsenic (A) versus dimensionless thickness of the F-doped CdO electrode(X) for some fixed values of parameters and various values of $D_{[As]}$. The dotted lines represent analytical solution and solid lines represent the numerical simulation.

Table 6: Comparison between analytical values and numerical values in Fig. 6(b)

$I_{max} = 0.5, K_M = 0.35, d = 0.5, As_0 = 0.5$				
$D_{[As]}$	X	Numerical solution for A	Analytical solution for A	Absolute percentage error
0.5	0	.8904868474	.8681	2.514000905
	0.2	.8947838712	.8733072906	2.400197555
	0.4	.9077164117	.8889589247	2.06644793
	0.6	.9294092813	.9151432569	1.534956094
	0.8	.9600718361	.9520045048	0.840284133
	1	1	1	0
0.6	0	.8912	.8904868474	0.080021611
	0.2	.8955103255	.8947838712	0.081121823
	0.4	.9084595387	.9077164117	0.081800781
	0.6	.9301018414	.9294092813	0.074460674
	0.8	.9605259046	.9600718361	0.047272905
	1	1	1	0
Average percentage error				0.810047

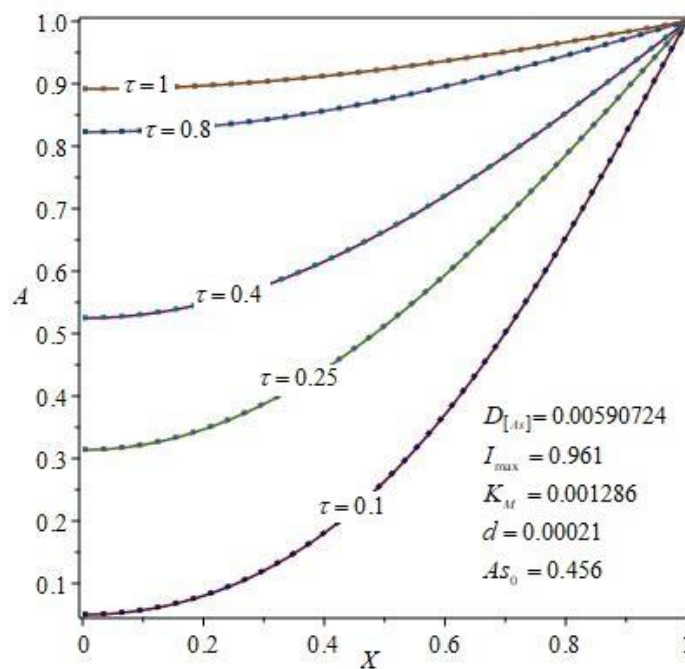


Fig. 7: Plot of dimensionless non-steady concentration of arsenic (A) versus dimensionless thickness of the F-doped CdO electrode(X) for experimental values of parameters [1] and various values of τ . The dotted lines represent analytical solution and solid lines represent the numerical simulation.

Table 7: Comparison between analytical values and numerical values in Fig. 7

$D_{[As]}=0.00590724, I_{\max}=0.961, K_M=0.001286, d=0.00021, A_{S_0}=0.456$				
τ	X	Numerical solution for A	Analytical solution for A	Absolute percentage error
0.1	0	.0500646368	.050724	1.317023836
	0.2	.0802550712	.08094726273	0.86248946
	0.4	.1806677101	.1814581805	0.437527215
	0.6	.3705127251	.3714387589	0.249933062
	0.8	.6537822931	.6547816664	0.152860258
	1	1	1	0
Average absolute percentage error				0.503306

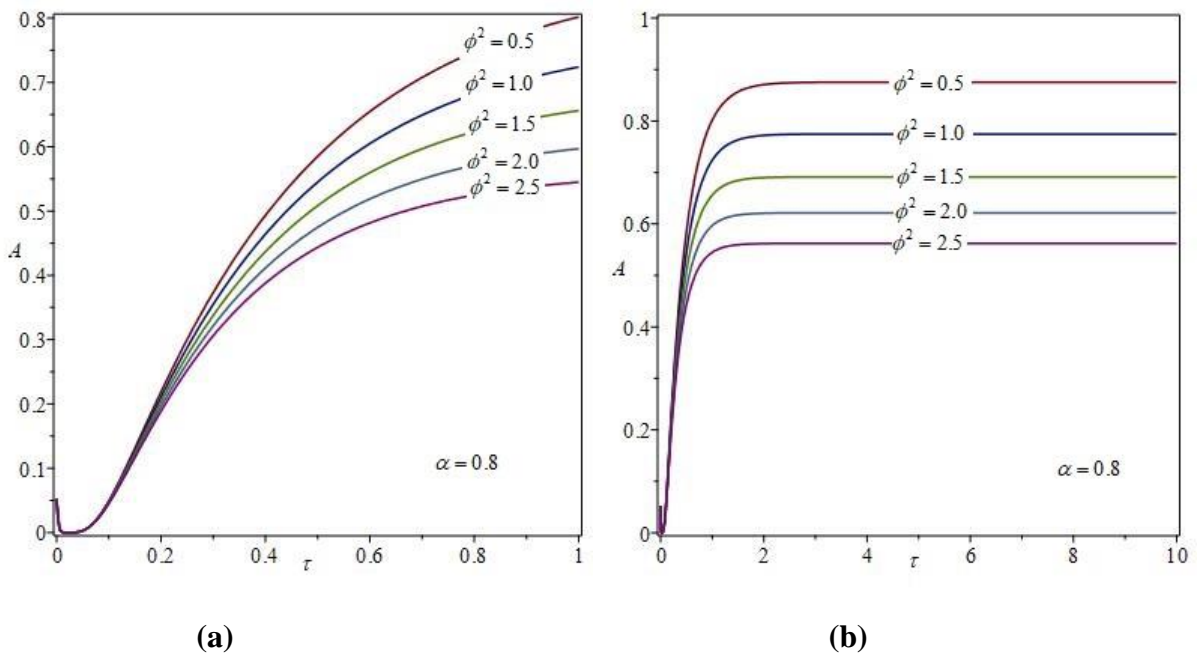


Fig. 8: (a) and (b): Plot of dimensionless concentration of arsenic (A) versus dimensionless time (τ) for various values of ϕ^2 .

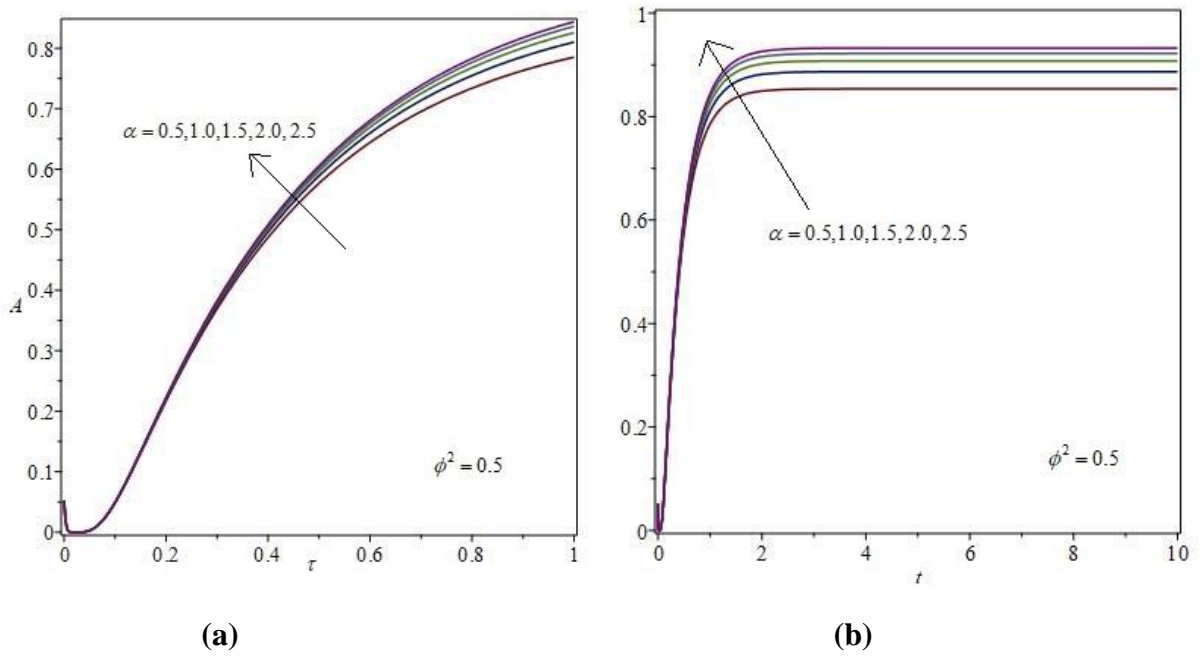


Fig. 9: (a) and (b): Plot of dimensionless concentration of arsenic (A) versus dimensionless time (τ) for various values of α .

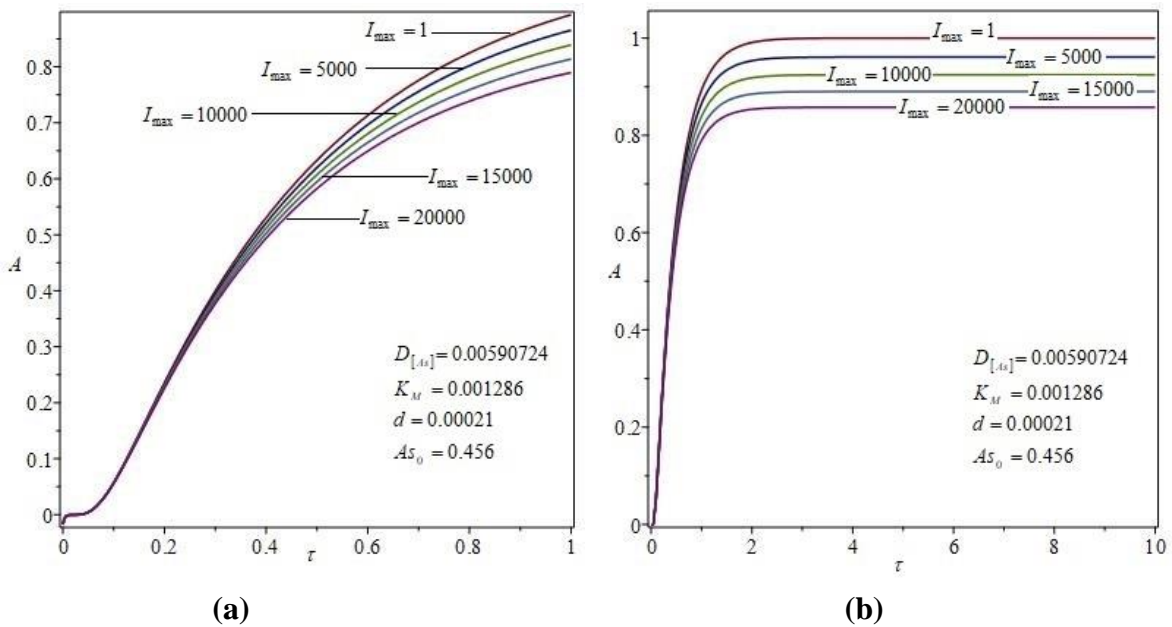


Fig. 10: (a) and (b): Plot of dimensionless concentration of arsenic (A) versus dimensionless time (τ) for various values of I_{max} .

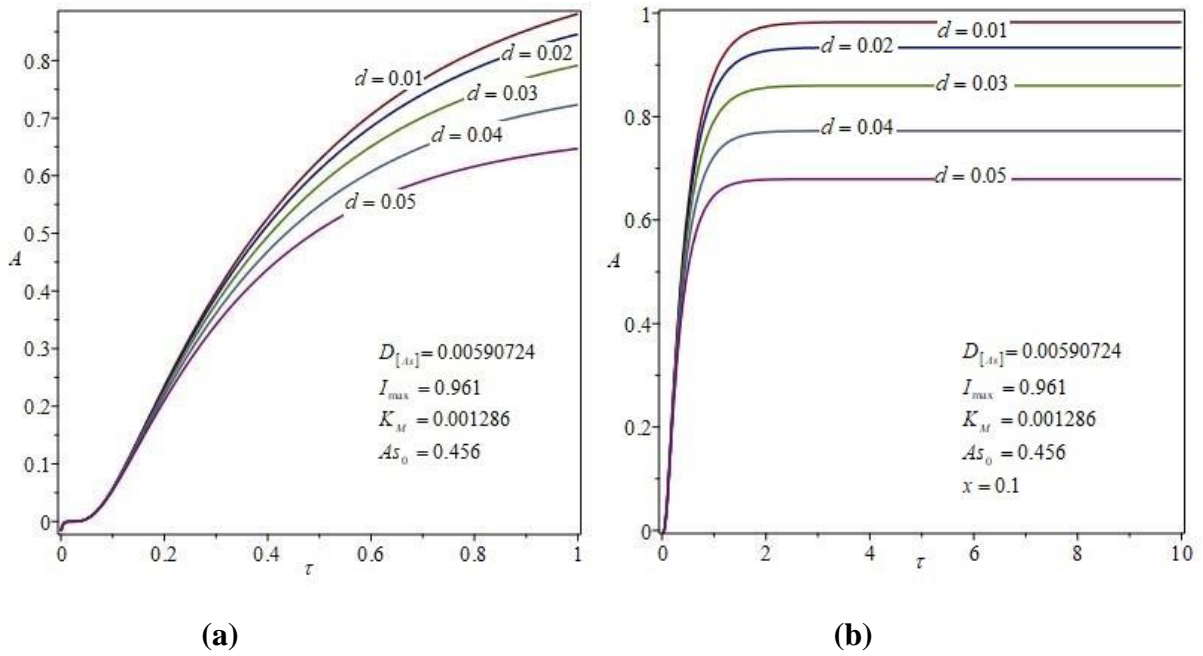


Fig. 11: (a) and (b): Plot of dimensionless concentration of arsenic (A) versus dimensionless time (τ) for various values of d .

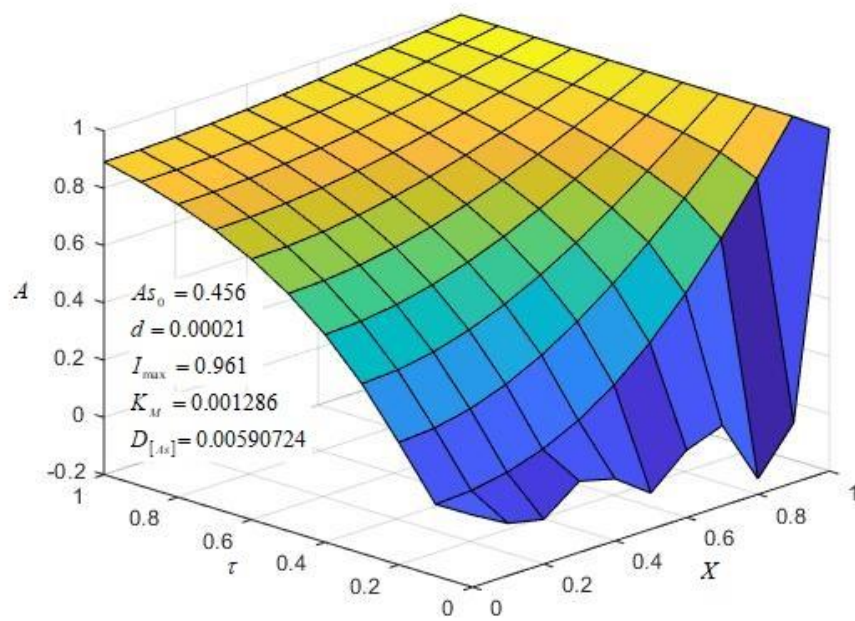


Fig. 12: The normalized 3-d dimensionless concentration of arsenic (A) versus dimensionless time (τ) and dimensionless thickness of the F-doped CdO electrode(X).

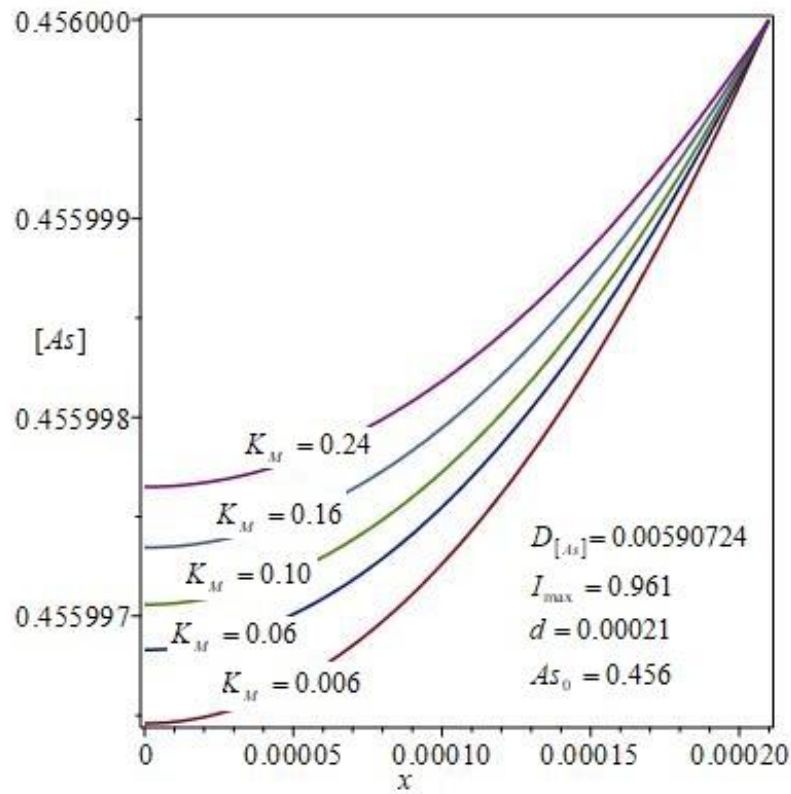


Fig. 13: Plot of arsenic concentration $[As]$ versus thickness of the F-doped CdO electrode (x) for various values of K_M .

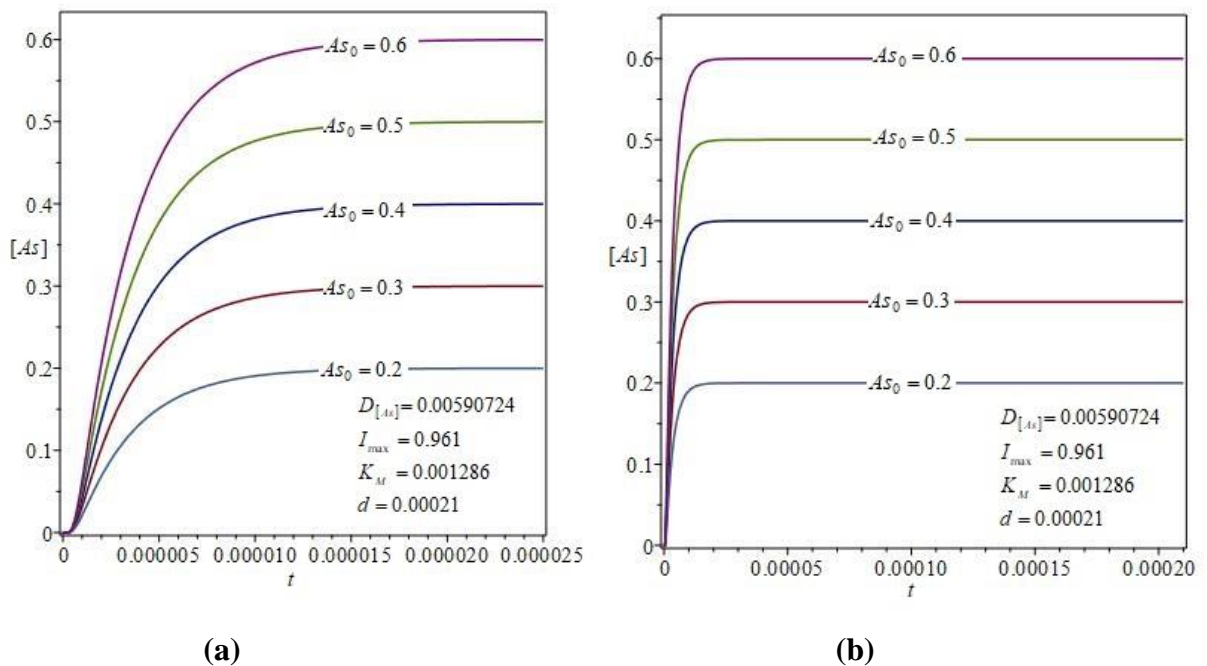


Fig. 14: (a) and (b): Plot of arsenic concentration $[As]$ versus time t for various values of As_0 .

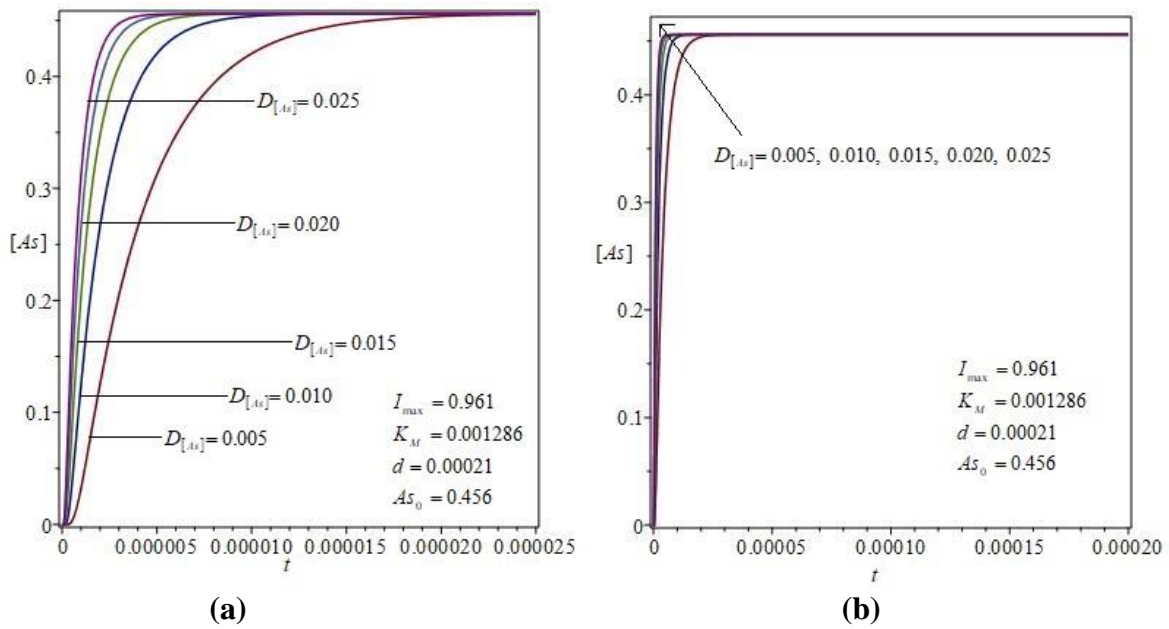


Fig. 15: (a) and (b): Plot of arsenic concentration $[As]$ versus time t for various values of $D_{[As]}$.

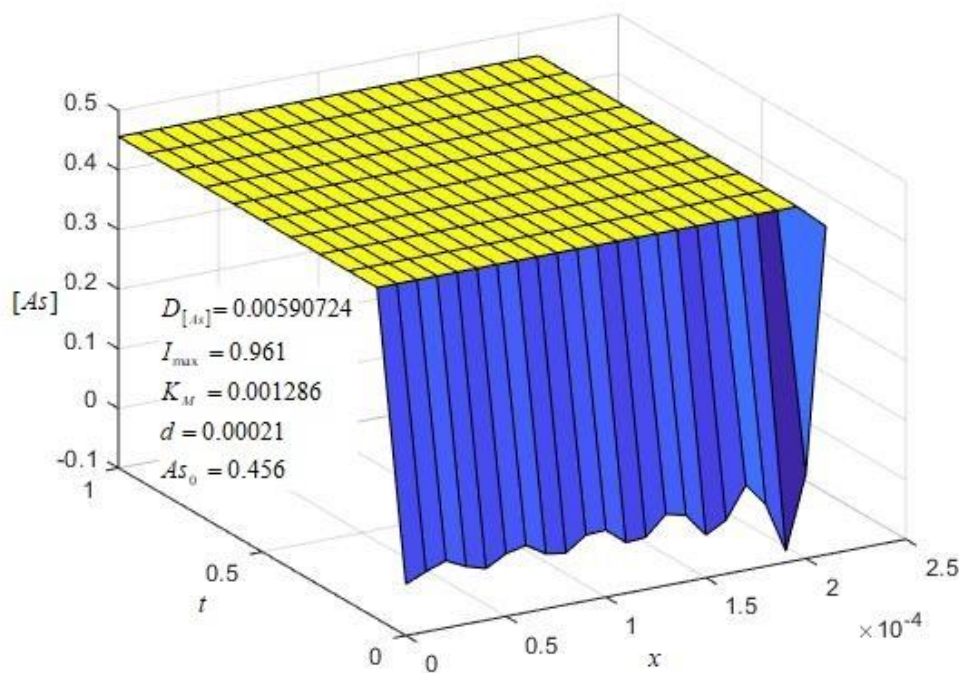


Fig. 16: The normalized 3-d arsenic concentration $[As]$ versus time t and thickness of the F-doped CdO electrode x .

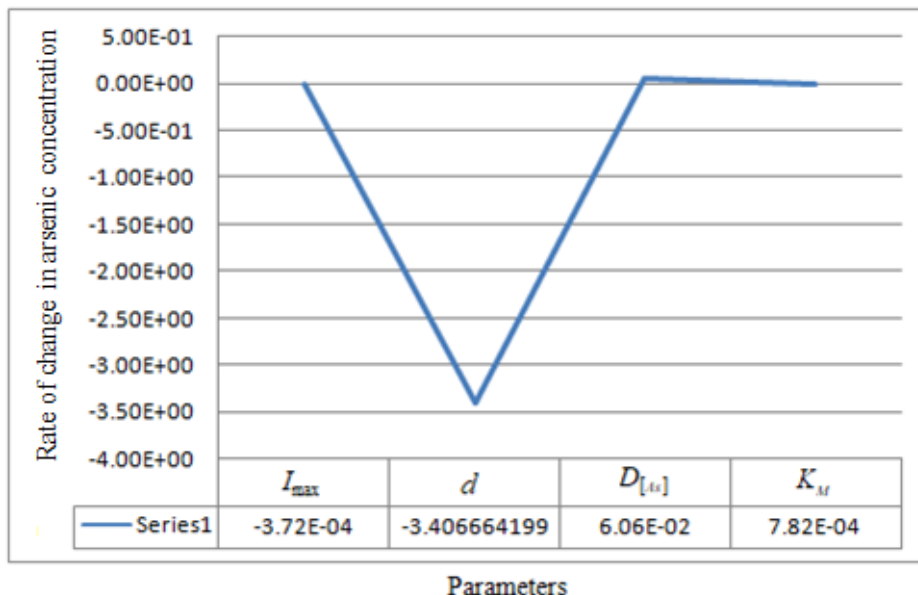


Fig. 17: Sensitive analysis of parameters

7. Results and Discussion

The steady state (Appendix A) and the non-steady state (Appendix B) analytical expressions for the arsenic concentration have been derived. The derived semi-analytical solutions are compared with the numerical solutions derived using Matlab in Figs. 1to7. The semi-analytical solutions make an excellent fit with the numerical solutions for experimental values of parameters[1].

Fig. 1 represents the dimensionless arsenic concentration (A) versus dimensionless spatial coordinate(X) for different values of parameter ϕ^2 . From the Figure it is clear to observe that the value of A decreases when the value of ϕ^2 increases. For different values of saturation parameter α , the dimensionless arsenic concentration (A) is depicted in Fig. 2. The figure clearly shows that A increases with increase in α .

Figs.3(a), 4(a), 5(a) and 6(a) illustrate the dimensionless arsenic concentration (A) for experimental values of parameters[1]and various values of $I_{max}, d, K_M, D_{[As]}$ respectively. From figures 3 to 6, we infer that A decreases with increase in I_{max} , decreases with increase in d , increases with increase in K_M and increases with increase in $D_{[As]}$.

Fig. 7 represents the arsenic concentration for various values of time for experimental values of parameters [1].The concentration increases when time increases. Figs.8 to 11 show the dimensionless arsenic concentration (A) versus dimensionless time τ for various values of ϕ^2, α, I_{max} and d respectively. Figs 13 to 15 show the arsenic concentration[As] versus time t for various values of K_M, As_0 and

$D_{[As]}$ respectively. From the figures, we observe that the system reaches steady state after $\tau = 2$. Fig. (12) shows the normalized three-dimensional dimensionless arsenic concentration (A) against dimensionless thickness of the F-doped CdO electrode (X) and dimensionless time τ . Fig. 16 shows the normalized three-dimensional arsenic concentration $[As]$ against thickness of the F-doped CdO electrode and time t .

Differential sensitivity analysis is based on partial differentiation of the aggregated model. We have found the partial derivative of arsenic concentration $[As]$ (dependent variable) with respect to the parameters I_{\max} , d , K_M , $D_{[As]}$ (independent variables). At some fixed experimental values ($D_{[As]} = 0.00590724$, $I_{\max} = 0.961$, $d = 0.00021$, $K_M = 0.001286$, $As_0 = 0.456$) of the parameters, numerical value of rate of change of arsenic concentration $[As]$ can be obtained. Sensitivity analysis of the parameters is given in Fig. 17. From this figure, it is inferred that $D_{[As]}$ has the maximum positive impact on the arsenic concentration $[As]$, while K_M accounts for only small positive change in arsenic concentration. d and I_{\max} both account for negative impact on arsenic concentration. d accounts for a larger change in arsenic concentration when compared to I_{\max} . This result is also confirmed in Fig. 17.

8. Conclusion

In this paper, steady state and time dependent approximate analytical expressions for the arsenic concentration $[As]$ are reported. The New Homotopy perturbation method is used to obtain the solution. Our results are of excellent fit with the numerical results. The obtained semi-analytical results under non-steady state will help the researchers to interpret the effect of the different parameters over the arsenic concentration in water.

References

- [1] D. Sathiyaseelan, M.B. Gumpu, N. Nesakumar, J.B.B. Rayappan, G. Hariharan, Wavelet based spectral approach for solving surface coverage model in an electrochemical arsenic sensor - An operational matrix approach, *Electrochimica Acta*, 2018.
- [2] Shiv Shankar, Uma Shanker, and Shikha, Arsenic contamination of groundwater: a review of sources, prevalence, health risks, and strategies for mitigation, *The Scientific World Journal*, 2014, Article ID 304524, 18 pages.
- [3] R. Baronas, F. Ivanauskas, J. Kulys, *Mathematical modeling of biosensors: An introduction for chemists and mathematicians*. Springer, Dordrecht, 2009.

- [4] V. Aseris, R. Baronas, J. Kulys, Computational modeling of bienzyme Biosensor with different initial and boundary conditions. *Informatica*, 24(2013): 505-521.
- [5] P. Ahuja, *Introduction to numerical methods in chemical engineering*. Texas Tech University Press, Lubbock, 2010.
- [6] A.M. Wazwaz, The variational iteration method for solving linear and nonlinear ODEs and scientific models with variable coefficients, *Central European Journal of Engineering*, 4(2014): 64-71.
- [7] A. Meena and L. Rajendran, Analysis of a pH-based potentiometric biosensor using the Homotopy perturbation method, *Chem. Eng. Technol*, 33(2010): 1999-2007.
- [8] M. Rasi, K. Indira and L. Rajendran, Approximate analytical expressions for the steady-state concentration of substrate and cosubstrate over amperometric biosensors for different enzyme kinetics, *Int. J. Chem. Kinet*. 45(2013): 322-336.
- [9] N. Mehala and L. Rajendran, Analysis of mathematical modelling on potentiometric biosensors, *ISRN Biochem.*, 2014: 1-11.
- [10] J. H. He, Homotopy perturbation method a new nonlinear analytical technique. *Applied Mathematics and Computations*, 135(2003): 73-79.
- [11] J. H. He, Homotopy perturbation technique, *Compt. Method, Appl. Mech. Eng.* 178(1999): 257-262.
- [12] J. H. He, A simple perturbation approach to Blasius equation, *Applied Mathematics and Computations*, 140(2003): 217-222.
- [13] J. H. He, Some asymptotic methods for strongly non-linear equations, *International of modern Physics*, B20(2006): 1141- 1199.
- [14] J. H. He, G C Wu, F Austin F, The variational iteration method which should be followed, *Non-linear Science Letters*, A(1)(2010):1- 30.
- [15] J. H. He, A Coupling method of a Homotopy technique and perturbation technique for non-linear problems, *International Journal of Non-linear Mechanics*, 35(2000): 37-43.
- [16] M MMousa, S F Ragab, Nurfosch, Application of the Homotopy perturbation method to linear and nonlinear schrodinger equations, *zeitschrift fur naturforschung*, 63(2008):140-144.
- [17] D Shanthi, V Ananthaswamy, L Rajendran, Analysis of non-linear reaction-diffusion processes with Michaelis-Menten kinetics by a new Homotopy perturbation method, *Natural Science*, 5(9)(2014): 1034.
- [18] V. Ananthaswamy, R. Shanthakumari, M. Subha, Simple analytical expressions of the non-linear reaction diffusion process in an immobilized biocatalyst particle using the new homotopy perturbation method, *review of bioinformatics and biometrics*, 3(2014): 22-28.

- [19] V. Ananthaswamy, C. Thangapandi, J. Joy Brieghti, M. Rasi and L. Rajendran, Analytical expression of nonlinear partial differential equations in mediated electrochemical induction of chemical reaction, *Advances in Chemical Science*, 4(7)(2014). 10.14355/sepacs.2015.04.002. (2015).
- [20] M. Rasi, L. Rajendran, and A. Subbiah, Analytical expression of transient current-potential for redox enzymatic homogenous system, *Sen. Actuat. B. Chem.*, B208(2015): 128-136.
- [21] M. Rasi, L. Rajendran and M. V. Sankaranarayanan, Transient current expression for oxygen transport in composite mediated biocathodes, *J. Elec. Chem. Soc.*, 162(9)(2015): H671-H680.
- [22] L. Rajendran, S. Anitha, Reply to Comments on analytical solution of amperometric enzymatic reactions based on HPM, *Electrochim. Acta* 102(2013): 474-476.
- [23] N. Mehala, L. Rajendran, Analysis of Mathematical modeling on potentiometric Biosensors, *ISRN Biochemistry*, 2014: 1-11.
- [24] V. Ananthaswamy, S. Narmatha, Comparison between the new Homotopy perturbation method and modified Adomian decomposition method in solving a system of non-linear self-igniting reaction diffusion equations, *International Journal of Emerging Technologies and Innovative Research* (www.jetir.org), 6(5)(2019): 51-59
- [25] S. Anitha, A. Subbiah, L. Rajendran, Analytical expression of non-steady –state concentrations and current pertaining to compounds present in the enzyme membrane of Biosensor, *The Journal of Physical chemistry*, 115(17)(2011): 4299- 4306.
- [26] Kara Asher, An introduction to Laplace transform, *international journal of science and research*, 2(1)(2013): 601-606.
- [27] Zhiqiang Zhou and Xuemei Gao, Laplace transform methods for a free boundary problem of time-fractional partial differential equation system, *Hindawi Discrete Dynamics in Nature and Society*, 2017: 1-9.

Appendix: A

In this appendix, we derive the steady state solution to eqns. (11) to (14) using New Homotopy perturbation method

The Steady state of eqns. (11) is

$$\frac{d^2 A}{dX^2} - \phi^2 \left(\frac{A}{\alpha + A} \right) = 0 \tag{A.1}$$

We construct the Homotopy for the eqn. (A.1) is as follows:

$$(1 - p) \left[\frac{d^2 A}{dX^2} - \phi^2 \left(\frac{A}{\alpha + 1} \right) \right] + p \left[\frac{d^2 A}{dX^2} - \phi^2 \left(\frac{A}{\alpha + A} \right) \right] = 0 \tag{A.2}$$

The approximate solution of eqn. (A.1) is

$$A = A_0 + pA_1 + p^2 A_2 + \dots \tag{A.3}$$

Substituting eqn. (A.3) in eqn. (A.1) and equating the coefficients of p^0 , we get

$$\frac{d^2 A_0}{dX^2} - \left(\frac{\phi^2}{\alpha + 1} \right) A_0 = 0 \tag{A.4}$$

The boundary conditions for the above equation becomes

$$X = 0, \frac{dA_0}{dX} = 0 \tag{A.5}$$

$$X = 1, A_0 = 1 \tag{A.6}$$

Solving the eqns. (A.4) to (A.6), we get

$$A = \frac{\cosh \frac{\phi}{\sqrt{\alpha + 1}} X}{\cosh \frac{\phi}{\sqrt{\alpha + 1}}} \tag{A.7}$$

Appendix: B

In this appendix, we derive the non-steady state solution to eqns. (11) to (14) using New Homotopy perturbation method

We construct the Homotopy for the eqn. (11) is as follows:

$$(1 - p) \left[\frac{\partial A}{\partial \tau} - \frac{\partial^2 A}{\partial X^2} + \phi^2 \left(\frac{A}{\alpha + 1} \right) \right] + p \left[\frac{\partial A}{\partial \tau} - \frac{\partial^2 A}{\partial X^2} + \phi^2 \left(\frac{A}{\alpha + A} \right) \right] = 0 \tag{B.1}$$

The approximate solution of eqn. (B.1) is

$$A = A_0 + pA_1 + p^2 A_2 + \dots \tag{B.2}$$

Substituting eqn. (B.2) in eqn. (B.1) and equating the coefficients of p^0 , we get

$$\frac{\partial A_0}{\partial \tau} - \frac{\partial^2 A_0}{\partial X^2} + \left(\frac{\phi^2}{\alpha + 1} \right) A_0 = 0 \tag{B.3}$$

The boundary conditions for the above equation becomes

$$X = 0, \frac{\partial A_i}{\partial X} = 0, i = 0, 1, 2, 3, \dots \tag{B.4}$$

$$X = 1, A_0 = 1, A_i = 0, i = 1, 2, 3, \dots \tag{B.5}$$

$$\tau = 0, A_i = 0, i = 0, 1, 2, 3, \dots \tag{B.6}$$

Applying Laplace transform to the eqns. (B.3) to (B.6), we get

$$\frac{\partial \bar{A}_0}{\partial \tau} - \frac{\partial^2 \bar{A}_0}{\partial X^2} + \left(\frac{\phi^2}{\alpha + 1} \right) \bar{A}_0 = 0 \tag{B.7}$$

$$X = 0, \frac{\partial \bar{A}_i}{\partial X} = 0, i = 0, 1, 2, 3, \dots \tag{B.8}$$

$$X = 1, \bar{A}_0 = \frac{1}{s}, \bar{A}_i = 0, i = 1, 2, 3, \dots \tag{B.9}$$

$$\tau = 0, \bar{A}_i = 0, i = 0, 1, 2, 3, \dots \tag{B.10}$$

Solving eqns. (B.7) to (B.10)

$$\bar{A}_0 = \frac{\cosh \sqrt{s + \frac{\phi^2}{\alpha + 1}} X}{s \cosh \sqrt{s + \frac{\phi^2}{\alpha + 1}}} \tag{B.11}$$

Now, let us invert eqn.(B.11) using the complex inversion formula.

If $\bar{y}(s)$ represents the Laplace transform of a function $y(\tau)$, then according to the complex inversion

formula $y(\tau) = \frac{1}{2\pi i} \oint_c \exp(s\tau) \bar{y}(s) ds$ where the integration has to be performed along a line $s = c$ in the

complex plane where $s = x + iy$. The real number c is chosen in such a way that $s = c$ lies to the right of

all the singularities, but is otherwise assumed to be arbitrary. In practice, the integral is evaluated by

considering the contour integral presented on the right-hand side of the equation, which is then evaluated

using the so-called Bromwich contour. The contour integral is then evaluated using the residue theorem.

In order to invert eqn.(B.11), we need to evaluate $\text{Re } s \left(\frac{\cosh \sqrt{s + \frac{\phi^2}{\alpha + 1}} X}{s \cosh \sqrt{s + \frac{\phi^2}{\alpha + 1}}} \right)$.

Now, finding the poles of $\overline{A_0}$ we see that there is a pole at $s = 0$ and there are infinitely many poles given

by the solution of the equation $\cosh\left(\sqrt{s + \frac{\phi^2}{\alpha + 1}}\right) = 0$

(ie) there are infinite number of poles at $s_n = -\frac{\phi^2}{\alpha + 1} - (2n + 1)^2 \frac{\pi^2}{4}$, where $n = 1, 2, 3, \dots$

Hence, we note that

$$L^{-1}(\overline{A_0}) = \operatorname{Re} s \left[e^{st} \left(\frac{\cosh\sqrt{s + \frac{\phi^2}{\alpha + 1}} X}{s \cosh\sqrt{s + \frac{\phi^2}{\alpha + 1}}} \right) \right]_{s=0} + \operatorname{Re} s \left[e^{st} \left(\frac{\cosh\sqrt{s + \frac{\phi^2}{\alpha + 1}} X}{s \cosh\sqrt{s + \frac{\phi^2}{\alpha + 1}}} \right) \right]_{s=s_n} \tag{B.12}$$

The first residue in eqn. (B.12) is given by

$$\operatorname{Re} s \left[\frac{\cosh\sqrt{s + \frac{\phi^2}{\alpha + 1}} X}{s \cosh\sqrt{s + \frac{\phi^2}{\alpha + 1}}} \right]_{s=0}$$

$$\lim_{s \rightarrow 0} s e^{st} \frac{\cosh\sqrt{s + \frac{\phi^2}{\alpha + 1}} X}{s \cosh\sqrt{s + \frac{\phi^2}{\alpha + 1}}} = \frac{\cosh\frac{\phi}{\sqrt{\alpha + 1}} X}{\cosh\frac{\phi}{\sqrt{\alpha + 1}}} \tag{B.13}$$

The second residue in eqn. (B.12) is given by

$$\operatorname{Re} s \left[e^{st} \left(\frac{\cosh\sqrt{s + \frac{\phi^2}{\alpha + 1}} X}{s \cosh\sqrt{s + \frac{\phi^2}{\alpha + 1}}} \right) \right]_{s=s_n}$$

$$= \lim_{s \rightarrow s_n} s e^{st} \frac{\cosh\sqrt{s + \frac{\phi^2}{\alpha + 1}} X}{\frac{d}{ds} \left(s \cosh\sqrt{s + \frac{\phi^2}{\alpha + 1}} \right)}$$

$$= \sum_{n=0}^{\infty} \frac{(-1)^{n+1} (2n + 1) \pi \cos\left(\frac{2n + 1}{2} \pi X\right) e^{-\left(\frac{\phi^2}{\alpha + 1} + \frac{(2n + 1)^2 \pi^2}{4}\right) \tau}}{\frac{\phi^2}{\alpha + 1} + \frac{(2n + 1)^2 \pi^2}{4}} \tag{B.14}$$

Using the eqns. (B.13) and (B.14) in an eqn.(B.12), we get

$$A_0 = \frac{\cosh\frac{\phi}{\sqrt{\alpha+1}} X}{\cosh\frac{\phi}{\sqrt{\alpha+1}}} + \sum_{n=0}^{\infty} \frac{(-1)^{n+1} (2n+1) \pi \cos\left(\frac{2n+1}{2} \pi X\right) e^{-\left(\frac{\phi^2}{\alpha+1} + \frac{(2n+1)^2 \pi^2}{4}\right) \tau}}{\frac{\phi^2}{\alpha+1} + \frac{(2n+1)^2 \pi^2}{4}} \tag{B.15}$$

From the eqn. (B.2), we get

$$A \approx A_0 = \frac{\cosh\frac{\phi}{\sqrt{\alpha+1}} X}{\cosh\frac{\phi}{\sqrt{\alpha+1}}} + \sum_{n=0}^{\infty} \frac{(-1)^{n+1} (2n+1) \pi \cos\left(\frac{2n+1}{2} \pi X\right) e^{-\left(\frac{\phi^2}{\alpha+1} + \frac{(2n+1)^2 \pi^2}{4}\right) \tau}}{\frac{\phi^2}{\alpha+1} + \frac{(2n+1)^2 \pi^2}{4}} \tag{B.16}$$

Appendix: C

MATLAB program to find the numerical solution of eqns. (11)-(14)

```
function pdex4
m = 0;
x = linspace(0,1);
t = linspace(0,0.8);
sol = pdepe(m,@pdex4pde,@pdex4ic,@pdex4bc,x,t);
u1 = sol(:,:,1);
figure
plot(x,u1(end,:))
title('u1(x,t)')
xlabel('Distance x')
ylabel('u1(x,2)')
%-----
function [c,f,s] = pdex4pde(x,t,u,DuDx)
c = [1];
f = [1] .* DuDx;
i=0.961;
k=0.001286;
d=0.00021;
D=0.00590724;
a0=0.456;
p=(i*d^2)/(a0*D);
a=k/a0;
```

```
F=-((p*u(1))/(a+u(1)));
s=[F];
% -----
function u0 = pdex4ic(x);
u0 = [0];
% -----
function [pl,ql,pr,qr] = pdex4bc(xl,ul,xr,ur,t)
pl = [0];
ql = [1];
pr = [ur(1)-1];
qr = [0];
```

Appendix: D

Nomenclature

Symbols	Meaning
$[As]$	arsenic concentration in μM
$D_{[As]}$	diffusion coefficient of arsenic in cm^2 / s
I_{max}	maximum current response in μA
K_M	Michaelis – Menten constant in μM
x	thickness of the F-doped CdO thin film electrode in cm
t	time in s
ϕ^2	Thiele modulus
α	saturation parameter
A	dimensionless arsenic concentration
X	dimensionless thickness of the F-doped CdO thin film electrode
τ	dimensionless time